Continuous Tuning of Electronic Correlations by Alkali Adsorption on Layered 1T-TaS_2

K. Rossnagel,[1,2,*] Eli Rotenberg,[2] H. Koh,[2] N. V. Smith,[2] and L. Kipp[1]

[1]*Institut für Experimentelle und Angewandte Physik, Universität Kiel, D–24098 Kiel, Germany*

[2]*Advanced Light Source, Lawrence Berkeley National Laboratory, Berkeley, California 94720, USA*

(Received 16 November 2004; published 16 September 2005)

Angle-resolved photoemission spectroscopy shows that a Mott-Hubbard type metal-insulator transition occurs at the Rb adsorbed surface of the layered charge-density-wave compound 1T-TaS_2. The transition is driven by adsorption induced modifications of the charge-density wave and of the interlayer coupling, leading to an increase of the on-site Coulomb correlation energy and a narrowing of the Ta 5d band perpendicular to the layers, respectively. The continuous rearrangement of spectral weight is measured live during the deposition process.

DOI: 10.1103/PhysRevLett.95.126403 PACS numbers: 71.30.+h, 71.45.Lr, 79.60.−i

Strongly correlated electron materials are expected to provide the basis of major new technologies by exploiting the interplay of charge, spin, and orbital degrees of freedom to produce complex new phases with useful properties [1]. The most prominent and widely studied example of such a new phase is the Mott-Hubbard insulating phase that results from a metallic band near half filling by changing the band filling n, the on-site Coulomb correlation energy U, or the one-electron bandwidth W [2]. Controlling these model parameters in real materials, however, is typically not so easy as it requires, e.g., the modification of the chemical composition [3] or the application of hydrostatic pressure [4].

In an ideal experiment one would directly probe the modifications of the electronic structure while tuning the crucial parameters U/W or n in the same crystalline sample without changing its chemical composition. Strikingly, *in situ* alkali adsorption on layered crystals, such as transition metal dichalcogenides (TMDCs), closely approaches the ideal experiment. Upon alkali deposition on layered TMDC surfaces two important effects are known to occur [5]. First, charge transfer from the adsorbed alkali atoms to the host lattice increases the band filling of the host material [6], and second, introduction of some alkali atoms between the layers decouples the topmost layers from the bulk, thus reducing the bandwidth perpendicular to the layers [7,8]. Remarkably, the adsorbed alkali atoms tend to form nanowire networks on the surfaces of TMDC compounds which produces large and pristine sample areas inside the meshes that are well separated from the alkali impurities forming the nanowires [9].

Among the many quasi-two-dimensional TMDCs 1T-TaS_2 is a special case since it exhibits an extraordinarily rich phase diagram showing a $\sqrt{13} \times \sqrt{13}$ charge-density wave (CDW) for $T < 540$ K which changes upon cooling from incommensurate to nearly commensurate and finally to commensurate with the underlying lattice [10]. Moreover, at the lock-in transition temperature of ≈ 180 K, a first order metal-insulator transition occurs with an in-plane resistivity increase of 1 order of magnitude. This transition can be understood as a Mott-Hubbard localization, caused by the favorable valence band structure created by the CDW and by the suddenly reduced screening of U when the domain boundaries are removed from the nearly commensurate phase [11,12].

Because of the peculiar interplay of long-range CDW order and local electronic correlations, there is every reason to expect pronounced changes of the electronic structure of 1T-TaS_2 upon alkali adsorption because alkali adsorption should affect the crucial parameters n and U/W directly or indirectly via modification of the CDW [13–15]. This expectation is further supported by recently observed metal-insulator transitions in the related compound 1T-$TaSe_2$ which were induced by the crystal surface [16] or by alkali intercalation [17,18]. However, in all of the previous alkali adsorption experiments [13–15,17,18] the intriguing evolution of the electronic structure near the Fermi level across the metal-insulator transition has not been investigated in great detail. For revealing such electronic structure changes, angle-resolved photoemission spectroscopy (ARPES) is the perfect tool as it probes not only electronic band dispersions but also the single-particle spectral function which contains many-body effects. Moreover, its surface sensitivity is ideal to investigate the electronic structure modifications that will naturally occur at the surfaces of layered materials when alkali atoms are adsorbed on them.

In this Letter we present spectroscopic evidence for a Mott-Hubbard type transition at the surface of 1T-TaS_2 induced by Rb adsorption. Exploiting the parallel detection capability of the photoelectron spectrometer, we map the evolution of the electronic structure of 1T-TaS_2 during the adsorption process and we demonstrate that the crucial parameter U/W can be *continuously* tuned through the critical value at which the Mott-Hubbard transition occurs. Our results provide detailed insight into the rearrangement of spectral weight across a metal-insulator transition that involves the interplay of local electronic correlations and strong electron-lattice interaction.

ARPES measurements were performed with a hemispherical analyzer (Gammadata SES-100) at beam line 7.0.1 of the Advanced Light Source. The photon energies used were in the range of 80–140 eV and the total energy resolution (photons plus electrons) was about 40 meV. Single crystal samples were grown by chemical vapor transport and clean surfaces were prepared by cleavage in ultrahigh vacuum. Rb was deposited *in situ* (during photoemission measurements) from a carefully outgassed SAES Getters source. The Rb evaporator was positioned about 6 cm away from the sample and operated at a current of 6 A. During the Rb evaporation, the pressure in the main chamber increased from 1×10^{-10} torr to 6×10^{-10} torr. All Rb deposition experiments were done at room temperature.

In pristine $1T$-TaS_2 the electronic structure near the Fermi level is governed by the lowest-lying Ta $5d$ band which is split into 3 subband manifolds by the $\sqrt{13} \times \sqrt{13}$ CDW. Two of the manifolds (carrying 6 electrons each per reconstructed unit cell) are completely filled and lie well below E_F; the third one (containing 1 electron) is half filled and defines the Fermi surface [11]. At the metal-insulator transition ($T_{\mathrm{MI}} \approx 180$ K) electronic correlations further split this band into the well-known lower and upper Hubbard subbands which in the following are assumed to be symmetrically located about E_F. The centroids of the two Hubbard bands are separated by $U \approx 0.3$–0.4 eV, but their tails show a very small overlap producing a deep pseudogap rather than a real gap [12,19,20].

Surprisingly, alkali adsorption on $1T$-TaS_2 generates a similar but much more pronounced scenario. Figure 1(a) shows the evolution of the valence band spectrum of $1T$-TaS_2 at the Γ point in the course of Rb deposition on the crystal surface. The sample was held at room temperature so that before the Rb deposition the system was rather far away from the temperature-induced Mott-Hubbard transition, as indicated by the high photoemission intensity at the Fermi level. Upon Rb deposition, the intensity at E_F continuously decreases, while simultaneously a signal located at about 0.5 eV below E_F appears. The progressive transfer of spectral weight away from E_F and the resulting opening of an energy gap is especially evident from the raw [Fig. 1(b)] and symmetrized [Fig. 1(c)] ARPES spectra taken at selected deposition times [21]. The corresponding Rb concentration has been determined from Rb $3d$ and Ta $4f$ core-level spectra, adding up appropriately weighted contributions of surface and subsurface Rb atoms. Error bars of the values given in Fig. 1 are in the order of 20%.

The photoemission spectra shown are qualitatively consistent with the spectral changes expected for a Mott-Hubbard transition [2,16,22]. Following this interpretation, the peak at the Fermi energy (before Rb deposition) can be identified as a quasiparticle feature whose spectral weight, in the course of Rb deposition, is continuously transferred to the lower and upper sidebands corresponding to the lower and upper Hubbard subbands. Two aspects of this transition are particularly noteworthy. First, the Mott-Hubbard localization induced by Rb adsorption is much stronger than the one occurring in pristine $1T$-TaS_2 at the temperature-induced metal-insulator transition. This is directly illustrated by the photoemission spectra taken from pristine $1T$-TaS_2 for the same experimental parameters but at a temperature of 30 K, i.e., deep in the Mott-Hubbard insulating phase [dotted lines overplotted in Figs. 1(b) and 1(c)]. Second, the energy separation between the lower and upper Hubbard band features continuously increases upon

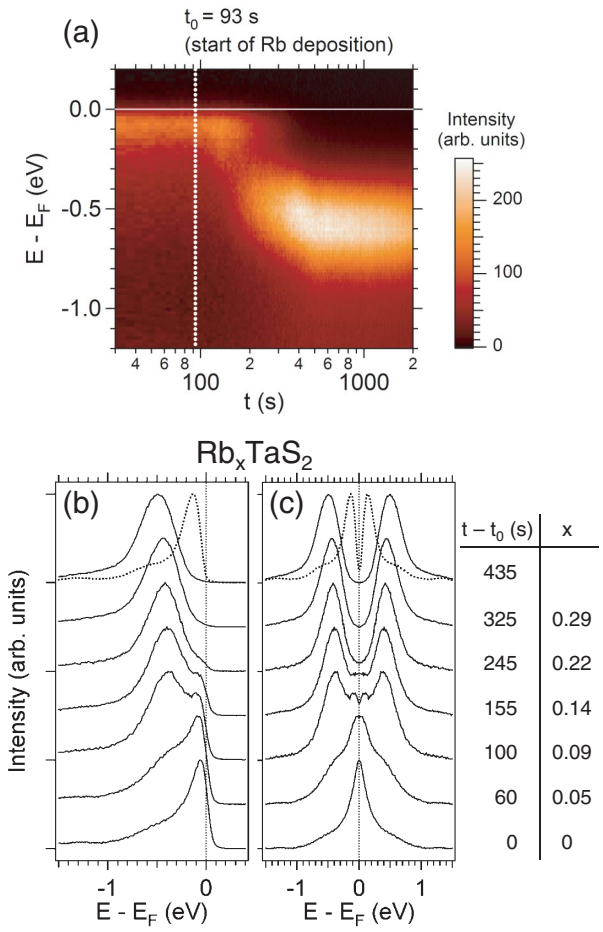

FIG. 1 (color online). (a) Photoemission intensity plot of the valence electronic structure of $1T$-TaS_2 at the Γ point as a function of Rb deposition time ($h\nu = 96$ eV, $T = 300$ K). (b) Valence band spectra at Γ for selected Rb deposition times and corresponding Rb concentration. (c) Same as (b), but spectra are symmetrized with respect to $E_F = 0$ [$I_{\mathrm{symm}}(\omega) = I_{\mathrm{raw}}(-\omega) + I_{\mathrm{raw}}(\omega)$]. Spectra in (a) and (b) originate from different deposition runs (each with a freshly cleaved crystal): (a) continuous deposition, (b) several short deposition cycles [with deposition times scaled to match peak shapes in (a)]. Spectra in (a) were taken in fixed-energy mode, whereas the energy was swept for the spectra in (b). In (a) and (b) low-temperature spectra of pristine $1T$-TaS_2 ($h\nu = 96$ eV, $T = 30$ K) are overplotted for comparison (dotted lines).

Rb adsorption from ≈ 0.6 eV to ≈ 1 eV [Fig. 1(c)], reflecting an equal increase in the on-site Coulomb interaction parameter U.

What causes the Mott-Hubbard transition in Rb/TaS_2? Figure 2 summarizes the changes of structural and electronic properties occurring during Rb deposition by comparing low-energy electron diffraction (LEED) images, Ta $4f$ core-level spectra, and ARPES intensity maps along certain high-symmetry directions taken *before* (left) and *after* (right) 250 s of Rb deposition. We will now discuss how the observed modifications of the geometric and electronic structure of $1T$-TaS_2 may affect the crucial parameters U, W, and n.

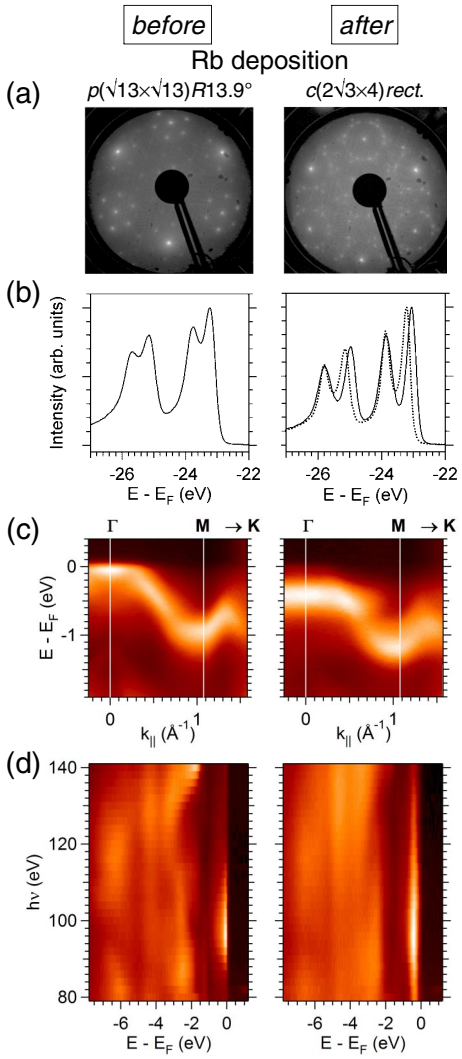

FIG. 2 (color online). Structural and electronic properties of $1T$-TaS_2 before (left) and after (right) 245 s of Rb deposition [cf. corresponding valence band spectra in Figs. 1(b) and 1(c)]. (a) LEED images ($E_{\mathrm{kin}} = 96$ eV). (b) Ta $4f$ core-level spectra ($h\nu = 96$ eV). A low-temperature ($T = 30$ K) spectrum of pristine $1T$-TaS_2 is overplotted on the right (dotted line). (c) ARPES intensity maps along the ΓMK lines ($h\nu = 96$ eV). (d) Normal emission spectra as a function of photon energy.

Modified CDW superlattice.—It was shown before that alkali deposition on $1T$-TaS_2 induces strong modifications of the CDW [13–15]. During Rb deposition, the CDW superlattice changes from the $p(\sqrt{13} \times \sqrt{13})R13.9°$ pattern of the nearly commensurate phase to a three-domain $c(2\sqrt{3} \times 4)$ rect. structure, as illustrated by the LEED images depicted in Fig. 2(a). The structural transition occurs between deposition times of 100 s and 155 s (see corresponding valence band spectra in Fig. 1). In addition, the Ta $4f$ core-level splitting, due to different electron densities at inequivalent Ta sites in the CDW pattern and proportional to the CDW amplitude [23], increases by about 300 meV [Fig. 2(b)]. The energy splitting after Rb deposition is again larger than the one in pristine $1T$-TaS_2 at a temperature far below T_{MI} [dotted line in Fig. 2(b) (right)].

Since the atomic displacements in the $c(2\sqrt{3} \times 4)$ rect. CDW phase have not been clarified yet and therefore no band structure calculations are available, we can only speculate about possible changes in the Ta $5d$ orbital overlap. Upon the transition from $p(\sqrt{13} \times \sqrt{13})R13.9°$ to $c(2\sqrt{3} \times 4)$ rect., the magnitude of the primitive translation vector is reduced from $\sqrt{13}$ to $\sqrt{7}$. Hence, under the assumption that still only one electron per reconstructed unit cell is involved in the metal-insulator transition, the orbital overlap between the relevant Ta atoms in neighboring clusters would become stronger leading to an increase of the in-plane bandwidth $W_{\|}$. However, a larger $W_{\|}$ would counteract the Mott-Hubbard transition.

A factor favoring the Mott-Hubbard localization is the observed increase of the on-site Coulomb correlation energy U, as measured by the energy separation between the Hubbard band features in Fig. 1(c). Since the energy gap between the Hubbard band features correlates with the Ta $4f$ core-level splitting during Rb deposition, we are tempted to conclude that U is directly related to the amplitude of the CDW; i.e., the long-range periodic modulations of the conduction electron density act locally to enhance correlation effects.

Unaltered band filling.—In pristine $1T$-TaS_2 the ellipsoidal Ta $5d$ Fermi surface pockets centered about the M and M' points are pseudogapped already at room temperature and the only true Fermi surface sheet is a small electron pocket centered at Γ [24–26]. This picture is confirmed by the ARPES intensity map along the ΓMK direction depicted in Fig. 2(c) (left). Upon Rb deposition, the final piece of Fermi surface is removed and no new Fermi surface sheet is created by population of unoccupied Ta $5d$ states [Fig. 2(c) (right)]. Hence, we may conclude that no or only a very small amount of Rb $5s$ electrons in the first stage of the adsorption process are transferred to the Ta $5d$ conduction band which therefore remains near half filling. The unchanged band filling may seem in contrast to Rb adsorption experiments on, e.g., $1T$-$TiSe_2$ and $1T$-$TiTe_2$ for which increased conduction band popula-

tions of up to 0.15 extra electrons per unit cell occur [27]. However, these systems are metallic and do not undergo metal-to-insulator transitions so that filling the lowest-lying unoccupied states is much easier because it does not cost an energy amount of order U.

Reduced interlayer coupling.—Alkali atoms adsorbed on layered TMDC surfaces tend to decouple the topmost sandwich layers from the bulk either by intercalation [7] or by the formation of nanowire networks [8]. The different mechanisms will not be discussed here. We only note that the band dispersions perpendicular to the layers (ΓA direction) are indeed flattened after Rb deposition [Fig. 2(d) (left) versus Fig. 2(d) (right)]. In particular, the interplane bandwidth $W_\perp$ of the relevant Ta $5d$ band just below E_F is reduced during Rb deposition. The importance of $W_\perp$ for the observed metal-insulator transition is corroborated by a recent band structure calculation for the $\sqrt{13} \times \sqrt{13}$ CDW phase of $1T$-TaS_2 [28]. This calculation shows that the CDW reconstruction induces a localization of the topmost occupied Ta $5d$ band within the plane and a strong delocalization out of plane. Hence, the bandwidth perpendicular rather than parallel to the layers appears as the crucial parameter for the Mott-Hubbard transition in Rb/TaS_2.

In conclusion, Rb deposition on the layered CDW compound $1T$-TaS_2 leads to an increase of the local Coulomb energy U via modification of the CDW and to a reduction of the bandwidth $W_\perp$ perpendicular to the layers through a decoupling of the topmost sandwich layers from the bulk. Employing these two effects, it becomes possible to continuously tune the $(U/W_\perp)$ ratio through the critical value for a Mott-Hubbard transition at the surface of $1T$-TaS_2. The concomitant spectral changes, which are directly observed by ARPES during the deposition process, provide detailed insight into the spectral properties of a metal-insulator transition. A theoretical description of this electronic transition involving strong electron-lattice coupling would be desirable.

Research at the University of Kiel is supported by the DFG Forschergruppe For 353. The Advanced Light Source is supported by the Director, Office of Science, Office of Basic Energy Sciences, Materials Sciences Division, of the U.S. Department of Energy under Contract No. DE-AC03-76SF00098 at Lawrence Berkeley National Laboratory. K. R. gratefully acknowledges support by the Alexander von Humboldt Foundation.

*Electronic address: rossnagel@physik.uni-kiel.de

[1] Y. Tokura, JSAP International **2**, 12 (2000).
[2] M. Imada, A. Fujimori, and Y. Tokura, Rev. Mod. Phys. **70**, 1039 (1998).
[3] J. S. Ahn, J. Bak, H. S. Choi, T. W. Noh, J. E. Han, Y. Bang, J. H. Cho, and Q. X. Jia, Phys. Rev. Lett. **82**, 5321 (1999).
[4] A. Husmann, J. Brooke, T. F. Rosenbaum, X. Yao, and J. M. Honig, Phys. Rev. Lett. **84**, 2465 (2000).
[5] R. H. Friend and A. D. Yoffe, Adv. Phys. **36**, 1 (1987).
[6] C. Ramírez and W. Schattke, Surf. Sci. **482-485**, 424 (2001).
[7] H. I. Starnberg, H. E. Brauer, L. J. Holleboom, and H. P. Hughes, Phys. Rev. Lett. **70**, 3111 (1993).
[8] R. Adelung, J. Brandt, K. Rossnagel, O. Seifarth, L. Kipp, M. Skibowski, C. Ramírez, T. Strasser, and W. Schattke, Phys. Rev. Lett. **86**, 1303 (2001).
[9] R. Adelung, L. Kipp, J. Brandt, L. Tarcak, M. Traving, C. Kreis, and M. Skibowski, Appl. Phys. Lett. **74**, 3053 (1999).
[10] J. A. Wilson, F. J. DiSalvo, and S. Mahajan, Adv. Phys. **24**, 117 (1975).
[11] P. Fazekas and E. Tosatti, Philos. Mag. B **39**, 229 (1979).
[12] F. Zwick, H. Berger, I. Vobornik, G. Margaritondo, L. Forró, C. Beeli, M. Onellion, G. Panaccione, A. Taleb-Ibrahimi, and M. Grioni, Phys. Rev. Lett. **81**, 1058 (1998).
[13] C. Pettenkofer and W. Jaegermann, Phys. Rev. B **50**, 8816 (1994).
[14] R. Adelung, J. Brandt, L. Kipp, and M. Skibowski, Phys. Rev. B **63**, 165327 (2001).
[15] H. J. Crawack and C. Pettenkofer, Solid State Commun. **118**, 325 (2001).
[16] L. Perfetti, A. Georges, S. Florens, S. Biermann, S. Mitrovic, H. Berger, Y. Tomm, H. Höchst, and M. Grioni, Phys. Rev. Lett. **90**, 166401 (2003).
[17] H. J. Crawack, Y. Tomm, and C. Pettenkofer, Surf. Sci. **465**, 301 (2000).
[18] S. E. Stoltz, H. I. Starnberg, and L. J. Holleboom, Phys. Rev. B **67**, 125107 (2003).
[19] B. Dardel, M. Grioni, D. Malterre, P. Weibel, Y. Baer, and F. Lévy, Phys. Rev. B **45**, R1462 (1992).
[20] B. Dardel, M. Grioni, D. Malterre, P. Weibel, Y. Baer, and F. Lévy, Phys. Rev. B **46**, 7407 (1992).
[21] Symmetrization of ARPES spectra about E_F removes the effects of the Fermi-Dirac and energy resolution function thus giving a direct view on the spectral function $A(\mathbf{k}, \omega)$, provided that $\mathbf{k} = \mathbf{k}_F$ and $A(\mathbf{k}_F, \omega) = A(\mathbf{k}_F, -\omega)$. Although the latter two conditions are not necessarily fulfilled here, the symmetrized spectra can still give a vivid idea of the spectral function.
[22] X. Y. Zhang, M. J. Rozenberg, and G. Kotliar, Phys. Rev. Lett. **70**, 1666 (1993).
[23] H. P. Hughes and J. A. Scarfe, Phys. Rev. Lett. **74**, 3069 (1995).
[24] M. Bovet, D. Popović, F. Clerc, C. Koitzsch, U. Probst, E. Bucher, H. Berger, D. Naumović, and P. Aebi, Phys. Rev. B **69**, 125117 (2004).
[25] Th. Pillo, J. Hayoz, H. Berger, R. Fasel, L. Schlapbach, and P. Aebi, Phys. Rev. B **62**, 4277 (2000).
[26] Th. Pillo, J. Hayoz, H. Berger, M. Grioni, L. Schlapbach, and P. Aebi, Phys. Rev. Lett. **83**, 3494 (1999).
[27] K. Rossnagel *et al.* (to be published).
[28] M. Bovet, S. van Smaalen, H. Berger, R. Gaal, L. Forró, L. Schlapbach, and P. Aebi, Phys. Rev. B **67**, 125105 (2003).